Journal of
Applied Crystallography
ISSN 0021-8898

Received 17 January 2011
Accepted 14 June 2011

A new approach for the determination of multiple cation locations and ordering, using the example of natural and heat-treated columbites

E. J. Kinast,[a,b] O. Isnard,[b]* J. B. M. da Cunha,[c] M. A. Z. de Vasconcellos[c] and C. A. dos Santos[c]

[a]Universidade Estadual do Rio Grande do Sul, Rua 7 de Setembro, 1156, 90010-191 Porto Alegre, Brazil, [b]Institut Néel, CNRS/Université J. Fourier, Avenue des Martyrs BP 166, 38042 Grenoble Cedex 9, France, and [c]Instituto de Física, Universidade Federal do Rio Grande do Sul, CP 15051, 91501-970 Porto Alegre, Brazil. Correspondence e-mail: olivier.isnard@grenoble.cnrs.fr

A new approach is proposed to determine unambiguously the location of four cations within the crystal structure of a natural AB_2O_6 columbite-type compound and derivatives, when submitted to order–disorder transitions caused by heat treatments. This method is based on the successive use of electron microprobe analysis to determine the cation concentration, Mössbauer spectroscopy to identify the Fe occupation, and a crystal structure determination of the samples combining Rietveld refinements of both neutron and X-ray diffraction. This approach is tested successfully to investigate (Fe, Mn, Nb, Ta) natural minerals as well as oxides obtained by heat treatment of the initial AB_2O_6 columbite-type compound.

1. Introduction

The mineral AB_2O_6 family, where A and B are inequivalent atomic positions occupied by cations including Fe, Mn, Co, Nb and Ta, exhibits two different behaviours which depend on the crystal structure symmetry. One, an orthorhombic solid solution, is named tantalite–columbite and the other, tetragonal, is named tapiolite (Hutton, 1958; Nickel *et al.*, 1963; Turnock, 1966; Wise & Cerny, 1996; Felten, 1967). The tantalite–columbites are sometimes referred to simply as columbite when the Nb content is larger than that of Ta, and tantalite when the Ta concentration is larger than that of Nb. The coexistence of phases in a natural tapiolite sample has been investigated by different techniques including Mössbauer spectroscopy, X-ray diffraction and microprobe analysis (dos Santos *et al.*, 2001; Kinast *et al.*, 2002; Tarantino *et al.*, 2003). These minerals are economically important since they are the major source of tantalum. In addition, they are very interesting from a fundamental point of view since they present interesting physical properties which have motivated numerous investigations in the past two decades (Eicher *et al.*, 1986; Wenger *et al.*, 1991; dos Santos & Oliveira, 1992; Kremer & Greedan, 1998; Mello *et al.*, 1999; Antonietti *et al.*, 2001; Eibschüt *et al.*, 1967; Drew *et al.*, 1993; Heid *et al.*, 1996; Beurlen *et al.*, 2008). Much fundamental research on the physical properties has also been performed on synthetic AB_2O_6 compounds (Felten, 1967; Esmaeilzadeh & Grins, 2002).

Studying the Mn–Ta–O ternary phase diagram, it was recently reported that the $MnTa_2O_6$ compound can exhibit, in addition to a stable tantalite structure, modifications related to the tri-rutile, wolframite and wodginite structures (Esmaeilzadeh & Grins, 2002). A year later, this polymorphism was found to be even richer with the discovery of a new high-temperature modification of $MnTa_2O_6$ (Tarakina *et al.*, 2003). The crystal structure of this last phase is incommensurately modulated. The studies of phase formation in the Mn–Ta–O system have shown them to have a more complex and varied crystal structure chemistry than originally expected. Furthermore, phases with tantalite-, tri-rutile (tapiolite)-, rutile- and wodginite-type structures are found in the Fe–MnTa–O system (Turnock, 1966). The different phases exhibit different crystal symmetry, resulting, in particular, from the differences in the cationic order. Indeed, in the crystal structure of the AB_2O_6-type compounds, the cations may occupy two different octahedral sites, A and B, with divalent cations preferring the A site and pentavalent cations preferring the B site. An order–disorder process allows intra-crystalline cation exchange between the A and B sites. Furthermore, it was found that in synthetic AB_2O_6 compounds, the cationic order within the octahedra is dependent upon the synthesis conditions and, in particular, upon the heat-treatment temperature (Tarantino *et al.*, 2003; dos Santos *et al.*, 1999).

It has been reported that, under heat treatment, columbite samples transform into different phases (wolframite, wodginite, ixiolite *etc.*) depending upon the initial composition and heat-treatment conditions. Some of these phases are structurally related to columbite. This is the case for wodginite, which, although retaining a different crystal structure symmetry and unit cell, exhibits similarities to the columbite structure. The relationship between the two structures is illustrated in Fig. 1. Concerning the cation layers, the ordered columbite presents an A-cation layer in between two B-cation

layers, along the *x*-axis direction. However, the ordered wodginite structure presents an alternated sequence of *B*-cation layers followed by an *AC* layer. Here, the *AC* layer is defined as a mixture of *A* and *C* cations in the plane.

These AB_2O_6 compounds are also actively investigated for their magnetic properties; the interest in these materials is motivated by their low-dimensional magnetic properties since they are considered as model compounds. Indeed, the MTa$_2$O$_6$ (M = Fe, Co, Ni) compounds present a two-dimensional antiferromagnetic behaviour (Eicher *et al.*, 1986; Kremer & Greedan, 1998; Kinast *et al.*, 2003, 2010; de Oliveira Neto *et al.*, 2007, 2008; Reimers *et al.*, 1989; Muraoka *et al.*, 1988), which has been extensively studied in the past few years, whereas the MNb$_2$O$_6$ series of compounds present a one-dimensional ferromagnetic chain antiferromagnetically coupled (Yeager, Morrish & Wanklyn, 1977; Yeager, Morrish, Wanklyn & Garrad, 1977; Kobayashi *et al.*, 1999, 2001; Hanawa *et al.*, 1994; Heid *et al.*, 1996; Sarvezuk *et al.*, 2011).

The synthesis, properties and applications of the columbite–niobates have been recently reviewed by Pullar (2009). He mentioned that the niobates–columbites are also attracting growing interest owing to their potential application as microwave ceramic substitutes for the highly expensive Ta-containing phases.

Order–disorder phenomena connecting these AB_2O_6 minerals have been extensively investigated (dos Santos *et al.*, 2001). In the context of the present discussion, a 100% ordered columbite means all the Fe and Mn atoms occupying the *A* site, and all the Ta and Nb occupying the *B* site. For many years, the degree of order in samples of the columbite type has often been qualitatively estimated from the values of the cell parameters *a* and *c* (Turnock, 1966; Wise *et al.*, 1985; Cerny *et al.*, 1986). For instance, Ercit *et al.* (1995) have performed a calibration of the degree of order as a function of these two lattice parameters, leading to an empirical formula for the (Fe,Mn)(Ta,Nb)$_2$O$_6$ system. This method is useful, but remains indirect and semi-quantitative with an estimated error of at least about 5%. The general trend is that the most disordered samples are those with the smaller *c*/*a* ratio. This simple rule of thumb is easy to use, but it has been demonstrated that it suffers from some exceptions and that some clearly disordered samples of the ixiolite type can be misidentified with ordered columbite. Consequently, Wenger *et al.* (1991) have considered that the single-crystal X-ray diffraction data should be used to differentiate between ixiolite and columbite. Other criteria have been tentatively established (dos Santos *et al.*, 2001) to estimate the degree of cation order in the (Fe,Mn)(Ta,Nb)$_2$O$_6$ system, but none have been found to be sufficient, leading to some mistakes being reported in the literature. This motivated us to develop our work on the analysis of selected natural compounds to combine different techniques aimed at probing, unambiguously, the degree of cation order.

In this article, we investigate the crystal structure of a columbite-type natural polycrystalline sample, combining several techniques in order to probe the degree of cation order. We will show that combining nuclear methods, like ^{57}Fe Mössbauer spectroscopy, with electron microprobe and diffraction techniques enables us to determine, unambiguously, the cation distribution within the crystal sites in the (Fe,Mn)(Ta,Nb)$_2$O$_6$-type columbite samples. We will present an investigation of the AB_2O_6 crystal structure by X-ray diffraction, neutron powder diffraction and a Mössbauer spectroscopy study of these polycrystalline compounds as-collected, as well as after heat treatment in air or in vacuum.

The combination of X-ray diffraction and neutron diffraction offers the advantage of being able to distinguish between Ta and Nb, whose electron numbers are significantly different (41 for Nb and 73 for Ta), whereas for the neutron case their coherent scattering length is almost identical. In contrast, the X-ray diffraction contrast between Fe and Mn is only one electron, whereas their neutron scattering lengths are opposite in sign, providing a relatively high contrast (Sears, 1992).

The article is organized as follows. §2 presents the experimental techniques and conditions used; in §3 we present successively the results of electron microprobe analysis, the ^{57}Fe Mössbauer spectroscopy investigation, and the X-ray and neutron diffraction techniques. Concerning the diffraction studies, the investigation of the as-collected natural samples is presented first, followed by a discussion of the influence of heat treatment on the crystal structure and its cation ordering.

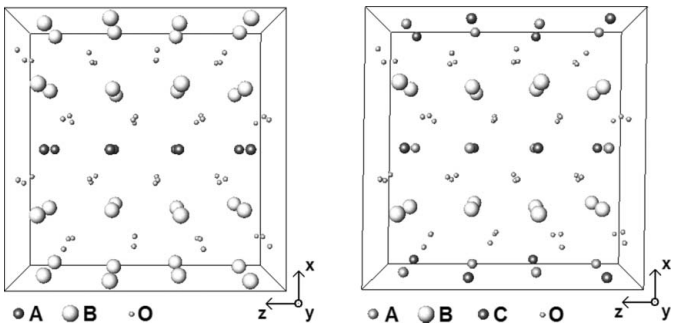

Figure 1
Crystal structure of the AB_2O_6-type columbite compounds (left) compared with the crystal structure of the ACB_2O_8-type wodginite compounds (right).

2. Experimental

The samples were polycrystalline pieces of columbite, selected from the Borborema pegmatite in the state of Paraiba, northeast Brazil (Adusumilli, 1976). A crystal fragment was powdered and submitted to two heat treatments: one part was heated in air, while the other was heated in vacuum ($P \simeq 10^{-5}$ Pa). In order to compare with earlier published results (Kinast *et al.*, 2002; dos Santos *et al.*, 1999), all the samples were heated at 1320 K for 48 h and subsequently slowly cooled at 15 K h^{-1}. This cooling rate has been retained since it is considered adequate for cation ordering, *e.g.* all the Fe + Mn in site *A* and all the Ta + Nb in site *B* of the orthorhombic or tetragonal AB_2O_6 structure types. The samples have been studied in three different states. They are distinguished by the codes N_{at}, A_{ir} and V_{ac} corresponding to the natural as-

collected state, and the heat-treated states after annealing in air or in vacuum atmosphere, respectively.

Electron probe microanalyses were performed on the as-collected sample with a wavelength dispersive microprobe system (CAMECA SX50). An accelerating potential of 15 keV, a beam current of 25 nA and a beam size of approximately 1 μm were used. Pure Nb ($L\alpha$), pure Ta ($L\alpha$), synthetic rutile (Ti $K\alpha$), natural olivine (Mn $K\alpha$–Fe $K\alpha$) and pure W (W $L\alpha$) were used as standards. The raw data were corrected online for drift, dead time and background. The formula was calculated on the basis of six oxygen atoms and taken from 20 analyses.

The purity of the phases was checked by X-ray diffraction using a Siemens D500 powder diffractometer in Bragg–Brentano geometry, with Cu $K\alpha$ radiation, $\lambda(K\alpha_1) = 1.54056$ Å and $\lambda(K\alpha_2) = 1.54439$ Å, a scan step of 0.02° and an angular 2θ range from 10 to 120°. An accurate determination of the lattice parameters was obtained by a least-squares refinement method.

The neutron diffraction experiments were performed at the Institut Laue–Langevin, Grenoble, France, on the D1B instrument. During the neutron diffraction measurements a cylindrical vanadium sample holder of 6 mm inner diameter was used. The room-temperature diffraction pattern has been recorded over an angular range of 80° (2θ) using a multi-detector with a step of 0.2° between each of the 400 ^{3}He detection cells. In this configuration, D1B operates with a wavelength of $\lambda = 1.28$ Å, selected by a (311) Bragg reflection of a Ge monochromator, and the take-off angle is 44.2° in 2θ.

The X-ray and neutron powder diffraction data were analysed with the Rietveld structure refinement program *FULLPROF* (Rodriguez-Carvajal, 1993).[1] The neutron scattering lengths used were $b_{Fe} = 0.945 \times 10^{-14}$ m, $b_{Mn} = -0.373 \times 10^{-14}$ m, $b_O = 0.5803 \times 10^{-14}$ m, $b_{Ta} = 0.691 \times 10^{-14}$ m, $b_{Nb} = 0.7054 \times 10^{-14}$ m [values taken from Sears (1992)].

For the Mössbauer spectroscopy measurements, absorbers with 50 mg of ground (320 mesh) material were prepared in order to satisfy the ideal absorber thickness approximation (Long *et al.*, 1983). The spectra were obtained at room temperature and 80 K using a constant acceleration electromechanical drive system with a multichannel analyser for collecting and storing the data. The hyperfine parameters were obtained by a least-squares procedure assuming Lorentzian line shapes. ^{57}Co in rhodium was used at room temperature as a source with a nominal activity of 50 mCi. A high-purity Fe metal foil was used for velocity-scale calibration.

3. Results and discussion

3.1. Electron microprobe analysis

The chemical composition of the as-collected sample has been derived from the microanalysis. The natural sample can be considered as homogeneous according to the composition analysis, which was performed in several places in the sample, as well as the backscattered electron images. This has been confirmed since the concentrations obtained in the 20 points probed were found to be very close. It is worthwhile mentioning that the sample exhibits a larger iron content in comparison to Mn. The sample is also richer in Ta compared with the Nb content. The concentration obtained is typical of columbite compounds. A result consistent with the X-ray diffraction results is discussed below. It was necessary to check for the occurrence of other cations such as Sn, W or Ti, which have been reported to be sometimes present in natural tantalite or columbite minerals. The presence of W in the sample can be excluded according to the microanalysis performed using the $L\alpha$ radiation. Traces of Ti have been observed for a concentration of about one weight percent, or less, depending on the probed area. An even lower content of Sn (below 0.5 wt%) has been observed in some limited regions, corresponding, most probably, to traces of SnO_2 as an inclusion. To conclude, based on this electron microprobe study, the formula $Fe_{0.60}Mn_{0.40}Ta_{1.3}Nb_{0.7}O_6$ can be proposed.

3.2. Mössbauer spectroscopy analysis

The ^{57}Fe Mössbauer spectroscopy technique enables us to adequately investigate order–disorder transitions in this kind of material. Hyperfine interactions are very sensitive to change in the near-neighbour environment and can discriminate the site location of Fe ions in columbite-like samples. Another advantage is that the analysis by Mössbauer spectroscopy is simpler if we want to distinguish between ixiolite and columbite phases, because in the former material Fe is in the 3+ valence state, whereas in the latter compound it is in the 2+ valence state (Bancroft, 1973).

For the as-collected natural sample, each Mössbauer spectrum has been fitted with two quadrupole doublets (ΔE_Q), both attributed to Fe^{2+} in different octahedrally coordinated sites. The site assignment has been done following earlier publications (dos Santos *et al.*, 1999, 2001; Bancroft, 1973) based on the correlation between the quadrupole splitting with the octahedral distortions. Indeed, the distortion of the octahedron has been investigated on partially ordered single-crystal $(Fe_{0.65}Mn_{0.30}Ti_{0.05})(Nb_{0.75}Ta_{0.25})_2O_6$ (Wenger *et al.*, 1991) or Fe–Mn$(Nb_{0.95}Ta_{0.05})_2O_6$ columbite samples (Tarantino *et al.*, 2003). Studying the octahedral edge length distortion (ELD), Griffen & Ribbe (1979) have reported that the FeO_6 octahedra are more distorted (ELD $\simeq 5$) than the NbO_6 ones (ELD $\simeq 3$). We, consequently, attribute the outer doublets to the large ΔE_Q (about 2–3 mm s^{-1}) owing to the Fe^{2+} in NbO_6 octahedra, while the inner one (ΔE_Q about 1.5 mm s^{-1}) is attributed to Fe^{2+} in the most distorted FeO_6 octahedra. Typical Mössbauer spectra are presented in Figs. 2 and 3 for the as-collected and the heated-in-air samples, respectively.

The disappearance of the outer quadrupolar doublet suggests that after the heat treatment all the Fe ions are in the 4*c* Wyckoff position (*A*-type octahedra). After heating the

[1] Supplementary material for this paper is available from the IUCr electronic archives (Reference: CG5181). Services for accessing these data are described at the back of the journal.

Table 1
Hyperfine parameters for the as-collected sample.

ΔE_Q is the quadrupole splitting at the iron sites; δ is the isomer shift relative to α-Fe; $\Gamma \pm 0.01$ mm s^{-1} is the line width at half-height; the typical uncertainty on the last figures is reported in parentheses.

T (K)	ΔE_Q (mm s^{-1})	δ (mm s^{-1})	Γ (mm s^{-1})	A (%)	Site assignment
300	1.65 (2)	1.14 (5)	0.52 (1)	55	FeO_6
	2.38	1.1	0.41	45	NbO_6
80	2.29	1.2	0.58	58	FeO_6
	2.76	1.24	0.32	42	NbO_6

Table 2
Hyperfine parameters for the sample heat treated in vacuum at 1323 K.

ΔE_Q is the quadrupole splitting at the iron sites; δ is the isomer shift relative to α-Fe; $\Gamma \pm 0.01$ mm s^{-1} is the line width at half-height; the typical uncertainty on the last figures is reported in parentheses.

T (K)	ΔE_Q (mm s^{-1})	δ (mm s^{-1})	Γ (mm s^{-1})	A (%)	Site assignment
300	1.60 (1)	1.17 (5)	0.35 (2)	96 (5)	FeO_6 or A type
	3.0	1.1	0.27	4 (5)	NbO_6 or B type
80	2.30 (1)	1.30 (5)	0.38 (2)	100	FeO_6
				0	NbO_6

sample in air, a dramatic change of the quadrupolar splitting is observed, leading to much smaller values below 1 mm s^{-1}. This is an indication of significant change at the iron sites and can be ascribed to oxidation of iron during the heat treatment in air. Indeed, ΔE_Q values are known to be much smaller for Fe^{3+} than for Fe^{2+} (Long *et al.*, 1983). Consequently, the Mössbauer values reported in Tables 1–3 can be divided into different categories: at room temperature $\Delta E_Q \simeq 0.55$ mm s^{-1} and $\Delta E_Q = 1.5$ mm s^{-1} are attributed to the Fe^{3+} and Fe^{2+} states at FeO_6 octahedra, respectively, while $\Delta E_Q \simeq 0.55$ mm s^{-1} and $\Delta E_Q \simeq 2.5$ mm s^{-1} are attributed to the Fe^{3+} and Fe^{2+} states at $(Nb/Ta)O_6$ octahedra, respectively. This assignment is confirmed by studies reported earlier on synthetic ferrocolumbite samples (Eibschüt *et al.*, 1967; Yeager, Morrish & Wanklyn, 1977; Yeager, Morrish, Wanklyn & Garrad, 1977; Zawislak *et al.*, 1995, 1997) where ΔE_Q up to $\sim$3 mm s^{-1} has been reported. The fit of the spectra recorded for the observed spectrum leads to significantly broadened lines in comparison to the instrumental resolution. According to the X-ray or neutron diffraction investigations discussed below, these broad lines do not come from a poor crystalline character of the studied samples, but rather indicate disorder in the extracted samples.

Table 3
Hyperfine parameters for the sample heat treated in air at 1323 K.

ΔE_Q is the quadrupole splitting at the iron sites; δ is the isomer shift relative to α-Fe; $\Gamma \pm 0.01$ mm s^{-1} is the line width at half-height; the typical uncertainty on the last figures is reported in parentheses.

T (K)	ΔE_Q (mm s^{-1})	δ (mm s^{-1})	Γ (mm s^{-1})	A (%)	Site assignment
300	0.49 (1)	0.40 (1)	0.33	100	FeO_6 or A type
80	0.50 (1)	0.51 (1)	0.33	100	FeO_6

The hyperfine parameters derived from the fit of the Mössbauer spectra were recorded for the as-collected sample and after heat treatement in vacuum, and are listed in Table 2. It is clear that the values obtained for the isomer shift and the quadrupole splitting are close to those corresponding to the A-type octahedral site indicating the quasi-exclusive presence of iron in the Fe^{2+} state on this octahedral position in the sample heat treated in vacuum. In particular, the quadrupole splitting is almost identical to that obtained for the A-type site in the natural sample. This result is true at both liquid-nitrogen and room temperature. The lines assigned to the B site, normally occupied by the Nb atoms, have completely disappeared after the heat treatment in vacuum in the pattern recorded at 80 K. This is proof of the ordering of the iron atoms during annealing. The room-temperature data present only traces (at most, a few percent) of Fe on the B site. Such a contribution has not been observed for the low-temperature data, demonstrating that the Fe cations are completely

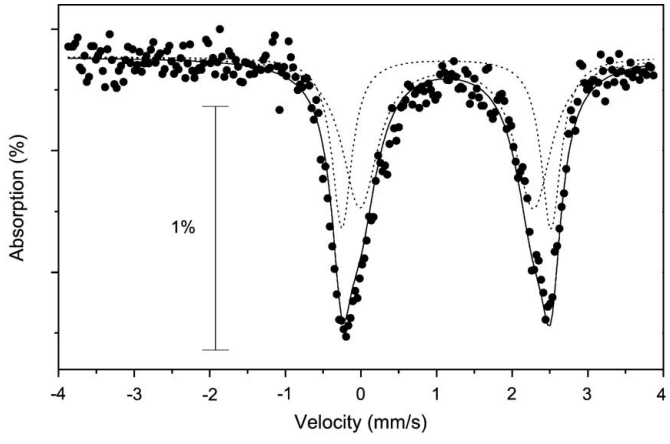

Figure 2
Mössbauer spectrum taken at 80 K for the as-collected natural sample. Circles represent the observed data. The solid line represents the calculated spectra based on a least-squares procedure. The dashed lines represent the calculated subspectra.

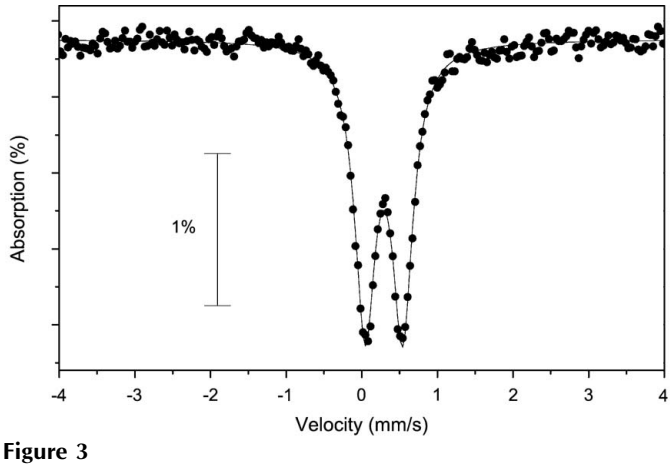

Figure 3
Mössbauer spectrum taken at room temperature for the natural sample heat treated in air. Circles represent the observed data and the solid line represents the calculated unique spectrum based on a least-squares procedure.

Table 4
Percentage of iron atoms on each of the two inequivalent octahedral cationic sites in the columbite structure as obtained from Mössbauer spectroscopy investigation.

Sample	%Fe on site *A* or *C*	%Fe on site *B*
N_{at}	55 site *A*	45
A_{ir}	100 site *A*	0
V_{ac}	100 site *C*	0

ordered or very close to completely ordered. The iron fractions on each site are shown in Table 4.

As can be seen from a comparison of the Mössbauer results (Tables 1–3), both ΔE_Q and δ_{IS} are strongly reduced upon heat treatment of the natural samples, bearing witness to the iron valence change from the divalent to the trivalent state occurring during the heat treatment in air. Another characteristic feature of the sample heat treated in air is that its Mössbauer spectra present only one doublet, indicating that the cation ordering has been completed. Accordingly, a good fit is obtained with the hyperfine parameters reported in Table 3.

The Γ value obtained after heat treatment is typically 0.3 mm s^{-1}, a value close to the instrumental resolution of 0.26 mm s^{-1} as obtained on the fit of the α-Fe foil reference used for calibration of the Mössbauer spectrometer. As will be apparent below, the observation of a good Fe-cation order by Mössbauer spectroscopy does not necessarily imply the presence of only one crystalline phase in the sample, but rather, an exclusive location of the Fe ions in the octahedral position devoted to the 3*d* transition metal ions.

3.3. Neutron and X-ray powder diffraction

3.3.1. Identification of the phases by X-ray diffraction. The different phases identified by Rietveld analysis of the room-temperature X-diffraction patterns are listed in Table 5(*a*), together with their corresponding lattice parameters. The indexing of the X-ray diffraction pattern reveals that the natural N_{at} sample exhibits only a single phase of *Pbcn* space group corresponding to an orthorhombic symmetry, typical of columbite phases. The phase concentrations and the goodness of fit of the Rietveld refinements are listed in Table 5(*b*) for all the studied compounds.

The X-ray diffraction pattern of the sample heat treated in vacuum is similar to the pattern of the original as-collected sample. The indexing of the Bragg peak corresponds to the presence of the columbite phase. This sample V_{ac}, being nearly a single phase, is reported in Tables 5(*a*) and 5(*b*) with a trace of rutile. Nevertheless, as can be seen from the comparison of the patterns given in Fig. 4, the intensities are significantly different from that of the as-collected N_{at} sample. Another noticeable difference is an expansion of the lattice parameters *a* and *b* upon annealing, whereas at the same time, the *c* parameter is reduced. As a consequence, the unit-cell volume of the columbite is only slightly increased from 416.5 to 417 Å^3 for the samples N_{at} and V_{ac}, respectively. These changes indicate that structural changes may occur upon annealing the samples.

Concerning the sample heat treated in air, A_{ir}, it is not a single phase anymore. According to the X-ray diffraction investigation, the A_{ir} sample is composed of a main phase of the ACB_2O_8 type exhibiting a wodginite crystal structure with minority phases of Ta_2O_5 and Nb_2O_5. This reveals that the sample has undergone oxidation during the heat treatment according to the reaction

$$2AB_2O_6 + \tfrac{1}{2}O_2 \rightarrow ACB_2O_8 + B_2O_5, \qquad (1)$$

where *A*, *B* and *C* represent inequivalent cation sites in the columbite AB_2O_6- and wodginite ACB_2O_8-type phases. These sites may be occupied by any of the Fe, Mn, Nb or Ta cations. The notation B_2O_5 refers to $(Ta,Nb)_2O_5$-type phases.

3.3.2. Rietveld analysis of the neutron and X-ray powder diffraction. The iron distribution on the different crystallographic sites has been fixed according to the Mössbauer spectroscopy results. Furthermore, as discussed above, the Ta and Nb cations are non-distinguishable by neutron diffraction. Consequently, the refinement of the neutron diffraction data has been used to refine the Mn occupancy on the different cation sites, as well as the (Nb + Ta)/Mn atomic ratio on each site. In other words, the cation sites have been supposed to be fully occupied and, after fixing the Fe content, the occupancies of the remaining sites by Mn or (Nb/Ta) have been refined. A further constraint was the overall (Nb + Ta)/Mn ratio according to the electron microprobe analysis. This refinement has been found to be very efficient since Mn and (Nb/Ta) have scattering lengths of opposite sign. In addition to the atomic occupancies, the atomic positions have been refined, leading to the results reported in Tables 6, 7 and 8 for the samples N_{at}, V_{ac} and A_{ir}, respectively.

As-collected natural sample (N_{at}). As can be seen from Fig. 5, the room-temperature neutron diffraction pattern of sample N_{at} can be fitted using only one phase of the columbite AB_2O_6

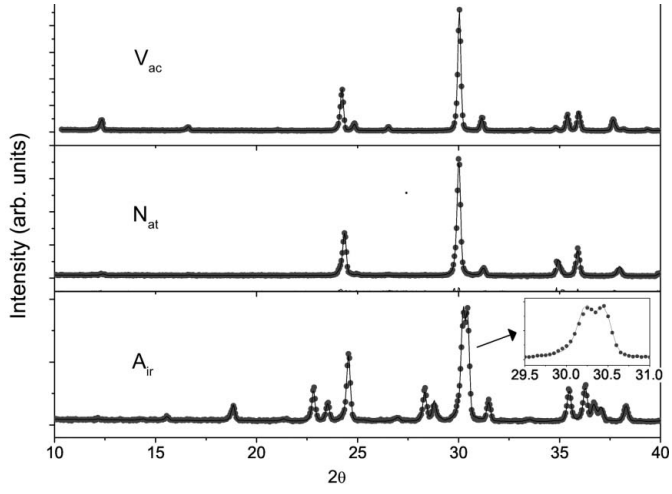

Figure 4
Comparison of the low-angle part of the X-ray diffraction patterns recorded at room temperature for three different states of the sample: as-collected columbite (N_{at}), and annealed at 1323 K either in air (A_{ir}) or in vacuum (V_{ac}).

Table 5
Crystallographic phases and Rietveld agreement factors according to the X-ray investigation of the natural samples in the as-collected state, after annealing in air or in vacuum atmosphere.

(*a*) Crystallographic phases. The standard deviations on the last figures are reported in parentheses.

Sample	Phases	Space group	*a* (Å)	*b* (Å)	*c* (Å)	*β* (°)	Volume (Å^3)
N_{at}	Columbite	*Pbcn*	14.199 (1)	5.7198 (4)	5.1288 (3)		416.55 (5)
V_{ac}	Columbite	*Pbcn*	14.326 (1)	5.7389 (3)	5.0718 (3)		416.97 (4)
	Rutile	$P4_2/mnm$	4.7488 (9)	4.7488 (9)	3.0678 (9)		69.18 (2)
A_{ir}	Wodginite	*C*2/*c*	9.4039 (8)	11.358 (8)	5.0614 (3)	90.564 (4)	540.60 (7)
	Ta_2O_5 type	*C*2*mm*	6.1966 (8)	3.6555 (4)	3.8933 (5)		88.19 (2)
	Nb_2O_5 type	*C*2/*c*	12.744 (8)	4.872 (3)	5.553 (4)	105.50 (6)	332.3 (4)

(*b*) Rietveld agreement factors (in %).

			X-ray			Neutron		
Sample	Phases	%	R_{wp}	R_B	R_{exp}	R_{wp}	R_B	R_{exp}
N_{at}	Columbite	100	12.4	12.4	6.56	12.5	8.47	2.37
V_{ac}	Columbite	99	16.0	7.71	9.93	7.86	4.67	1.68
	Rutile	1		10.8			11.4	
A_{ir}	Wodginite	80	17.9	7.73	12.5	14.5	6.98	1.41
	Ta_2O_5 type	12		11.2			17.1	
	Nb_2O_5 type	7		17.5			18.1	

type. In the as-collected state the cations are found to be disordered even if iron and manganese present a pronounced preference for the *A* site. In contrast, the *B* site is preferentially occupied by the Nb and Ta sites. The neutron refinement leads to an Mn content of 24% on the *A* site and 8.3% in the *B* position. The atomic positions obtained are listed, together with the refined atomic displacement parameter values, in Table 6. Rather large values of the atomic displacement parameters are observed for the cations; this most probably reflects disorder in the crystal structure of the natural sample. Since only a mean value of the niobium plus tantalum content can be obtained on each crystal site from the neutron powder diffraction data, their respective concentration has been determined from the refinement of the X-ray pattern. The X-ray pattern can be fitted very well – see Fig. 6 – starting from the results obtained from the neutron diffraction. During the X-ray analysis the Fe and Mn occupancies have been constrained to those deduced from Mössbauer spectroscopy and neutron diffraction analysis, respectively. As can be seen from Table 6, the values of the structural parameters deduced from the X-ray analysis are consistent with the values from neutron diffraction, confirming the quality of the structural model. The Ta atoms are found to fill one half of the *B* sites and the Nb atoms 28%, in excellent agreement with the expected preference for such a crystal position. In order to illustrate the cation locations, the chemical formula of sample N_{at} can be rewritten as $(Fe_{0.33}Mn_{0.24}Ta_{0.30}Nb_{0.13})$-$(Fe_{0.14}Mn_{0.08}Ta_{0.50}Nb_{0.28})_2O_6$.

At this point, it is interesting to compare our results with Ercit's order parameter (Ercit *et al.*, 1995). Using the lattice parameters given in Table 5(*a*), values of 11.5 and 93% (±5% at least) are obtained for the as-collected and heated-in-vacuum samples, respectively. Our experimental data confirm the tendency of Ercit's order parameter, while giving experimental quantitative occupancies for the cations and proving a complete ordering in the V_{ac} sample.

Natural sample heated in vacuum (V_{ac}). The neutron diffraction pattern of the natural sample heated in vacuum can be well reproduced taking into account the columbite *Pbcn* structure only (Fig. 7). For consistency with the X-ray investigation the presence of a trace of rutile has also been investigated, but the resultant amount from the refinement was not significant. The results of the Rietveld refinement are listed in

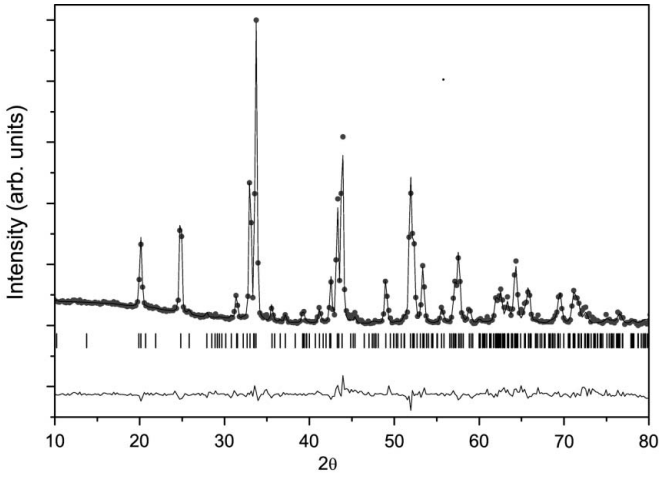

Figure 5
Rietveld refinement of the room-temperature neutron diffraction pattern recorded for the as-collected sample (N_{at}). The Bragg peak positions corresponding to the columbite structure (*Pbcn*) are indicated below by the row of ticks.

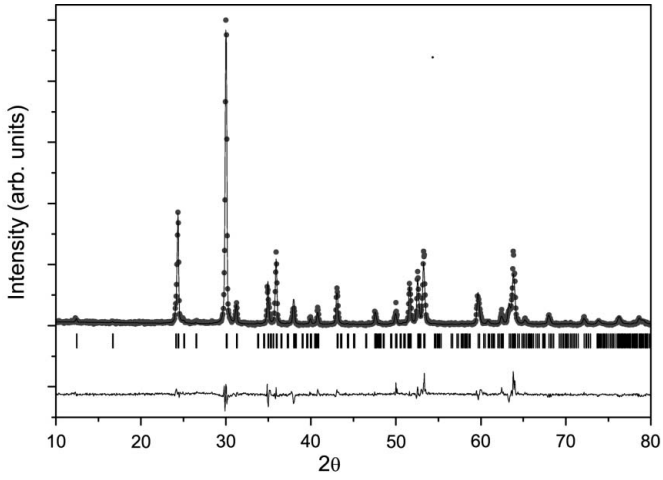

Figure 6
X-ray diffraction pattern recorded at room temperature for the as-collected sample (N_{at}). The points refer to the experimental data, the line to the Rietveld refinement fit. The Bragg peak positions corresponding to the structure of columbite (*Pbcn*) correspond to the row of ticks.

Table 6
Atomic positions and site occupancy (%) of the columbite structure (*Pbcn*) as obtained from the refinement of the X-ray (first row) and neutron (second row) diffraction patterns for the as-collected sample: $(Fe_{0.33}Mn_{0.24}Ta_{0.30}Nb_{0.13})(Fe_{0.14}Mn_{0.08}Ta_{0.50}Nb_{0.28})_2O_6$.

The standard deviations on the last figures are reported in parentheses.

Pbcn	Wyckoff position	*x*/*a*	*y*/*b*	*z*/*c*	*B* (Å^2)	Fe/Mn/Ta/Nb (%)
A	4*c*	0	0.343 (2)	1/4	0.5	33/24/30/13
		0	0.342 (6)	1/4	1.06 (6)	
B	8*d*	0.1650 (5)	0.1690 (9)	0.741 (1)	0.4 (1)	14/8/50/28
		0.165 (2)	0.167 (3)	0.750 (4)	1.06 (6)	
O1	8*d*	0.0924 (8)	0.102 (1)	0.059 (2)	0.5	
		0.089 (1)	0.109 (2)	0.062 (1)	0.51 (4)	
O2	8*d*	0.4225 (7)	0.129 (1)	0.075 (2)	0.5	
		0.422 (1)	0.111 (2)	0.087 (1)	0.51 (4)	
O3	8*d*	0.761 (1)	0.117 (1)	0.084 (2)	0.5	
		0.7582 (9)	0.132 (1)	0.101 (1)	0.51 (4)	

Table 7
Atomic positions and site occupancy (%) of the columbite structure (*Pbcn*) as obtained from the refinement of the X-ray (first row) and neutron (second row) diffraction patterns for the sample heated in vacuum: $(Fe_{0.60}Mn_{0.40})(Ta_{0.65}Nb_{0.35})_2O_6$.

The standard deviations on the last figures are reported in parentheses.

Pbcn	Wyckoff position	*x*/*a*	*y*/*b*	*z*/*c*	*B* (Å^2)	Fe/Mn/Ta/Nb (%)
A	4*c*	0	0.330 (1)	1/4	0.4	60/40/0/0
		0	0.325 (1)	1/4	1.1 (1)	
B	8*d*	0.1619 (8)	0.1790 (2)	0.745 (1)	0.4	0/0/65 (2)/35 (2)
		0.1726 (4)	0.172 (1)	0.763 (1)	0.7 (1)	
O1	8*d*	0.0811 (9)	0.119 (2)	0.068 (3)	0.5	
		0.0842 (3)	0.129 (1)	0.092 (1)	0.63 (3)	
O2	8*d*	0.4192 (8)	0.121 (2)	0.083 (3)	0.5	
		0.4279 (3)	0.113 (1)	0.081 (1)	0.63 (3)	
O3	8*d*	0.757 (1)	0.132 (2)	0.083 (2)	0.5	
		0.7592 (4)	0.102 (1)	0.075 (1)	0.63 (3)	

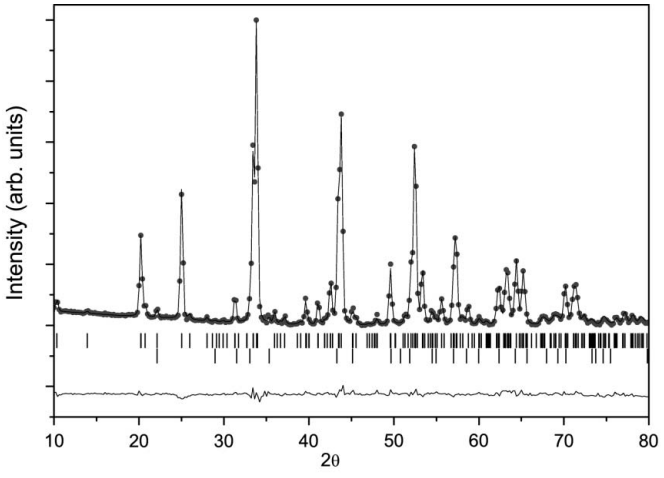

Figure 7
Rietveld refinement of the room-temperature neutron diffraction pattern recorded for the as-collected sample and for the natural sample heated in vacuum (V_{ac}). The points refer to the experimental data, the line to the Rietveld refinement fit. The Bragg peak positions corresponding to the structure of columbite (*Pbcn*) correspond to the first row of ticks. We also see the signatures of small amounts of rutile (second row of ticks).

Table 8
Atomic positions and site occupancy (%) of the wodginite structure (*C*2/*c*) as obtained from the refinement of the X-ray (first row) and neutron (second row) diffraction patterns for the sample heated in air: $(Mn_{0.61}Ta_{0.39})Fe(Mn_{0.06}Ta_{0.58}Nb_{0.36})_2O_8$.

The standard deviations on the last figures are reported in parentheses.

*C*2/*c*	Wyckoff position	*x*/*a*	*y*/*b*	*z*/*c*	*B* (Å^2)	Fe/Mn/Ta/Nb (%)
A	4*e*	0	0.6655 (8)	1/4	0.4	0/61 (3)/39 (3)/0
		0	0.665 (4)	1/4	0.5	
B	8*f*	0.253 (1)	0.4129 (2)	0.245 (1)	0.4	0/6 (3)/58 (3)/36 (3)
		0.2545 (2)	0.4185 (2)	0.261 (4)	0.5	
C	4*e*	0	0.1635 (3)	1/4	0.4	100/0/0/0
		0	0.164 (1)	1/4	0.5	
O1	8*f*	0.133 (2)	0.066 (2)	0.105 (1)	0.5	
		0.1377 (1)	0.0573 (1)	0.069 (3)	0.6	
O2	8*f*	0.139 (2)	0.432 (3)	0.569 (4)	0.5	
		0.131 (1)	0.443 (1)	0.582 (2)	0.6	
O3	8*f*	0.109 (2)	0.299 (3)	0.099 (8)	0.5	
		0.118 (1)	0.308 (2)	0.0934 (2)	0.6	
O4	8*f*	0.104 (4)	0.186 (2)	0.587 (3)	0.5	
		0.119 (1)	0.191 (1)	0.581 (2)	0.6	

Table 7. The atomic positions are typical of a columbite phase and do not vary much from those observed for the N_{at} sample discussed above. It is noticed that the estimated atomic displacement parameter on the *B* site is significantly smaller than for the sample N_{at}. This reduction most probably results from the ordering of the cations upon annealing the sample in vacuum. Indeed, site *B* is found to be exclusively occupied by Ta and Nb. The other site, *A*, is exclusively occupied by Fe and Mn atoms and the obtained occupancies are listed in Table 7. The neutron diffraction results were used as starting values to fit the X-ray diffraction pattern of sample V_{ac}. Then, the atomic parameters, as well as the occupancies of the Nb^{5+} and Ta^{5+} cations, were refined. The X-ray fit obtained (see Fig. 8) bears witness to the quality of the structural model. It is clear that annealing has led to the ordering of the cations. One can notice that the Fe, Mn, Nb and Ta contents not only enable us to fit Mössbauer spectroscopy and X-ray and neutron diffraction results consistently, but are also in agreement with the concentration measured by electron microprobe analysis – the 3*d* metal being only on *A* sites, whereas the Ta and Nb are exclusively located on the *B* sites. Taking into account the cation locations, the chemical formula of sample V_{ac} can be rewritten as $(Fe_{0.60}Mn_{0.40})(Ta_{0.65}Nb_{0.35})_2O_6$.

Natural sample heated in air (A_{ir}). For this sample, the Rietveld refinement of the room-temperature neutron diffraction pattern is plotted in Fig. 9. As can be seen from this figure, the sample has completely changed its crystal structure. The neutron analysis confirms the above deduction from X-rays, and the main phase is now of the wodginite type ACB_2O_8 (Ercit *et al.*, 1992; Ferguson *et al.*, 1976). Such a structure is shown in Fig. 1. The oxidation of the sample during annealing in an air atmosphere also led to the formation of Ta_2O_5- (Lehovec, 1964) and Nb_2O_5-type (Ercit, 1991) phases whose concentrations are listed in Table 8.

Following earlier studies on wodginite samples, we have assumed a strong preference for Fe^{3+} for the *C* position of

wodginite (dos Santos *et al.*, 1999, 2001; Ercit *et al.*, 1992). According to our Mössbauer spectroscopy discussed above, all the Fe atoms of this sample are located on the same type of cation sites. This fact rules out the possibility of having iron on the *A* site since only the Fe^{2+} cation can exist on this site. This assignment of the Fe atoms on the *C* position is in full agreement with results reported in the literature on natural or synthetic ferrocolumbite $(Fe,Mn)(Ta,Nb)_2O_6$ heated in air (Santos *et al.*, 1999) and on $(Mn,Fe)Ta_2O_8$ wodginite (Ercit *et al.*, 1992). Taking into account the change of Ta and Nb content to form Ta_2O_5 and Nb_2O_5 upon annealing in air, the cation content of the wodginite has been recalculated. Then, the same fitting procedure has been applied starting from the iron location on the *C* site to account exclusively for the Fe^{3+}-type Mössbauer spectrum, while the Mn location has been determined from the fit of the neutron data. As expected, a large preference of the Mn atoms for the *A* position of wodginite is obtained. The neutron fit could be slightly improved by placing traces of Mn on the *B* sites. This hypothesis has been checked against the X-ray pattern, which led to a very small Mn content (6%) on the *B* sites, a value barely significant. The possible location of Nb on the *A* site has been tested on the X-ray pattern, but the Rietveld refinement clearly indicates that only Mn and Ta are sitting on the *A* position. The refinement of the X-ray diffraction pattern (Fig. 10) led us to conclude that Nb is exclusively located on the *B* position, whereas the Ta atoms fill the remaining sites on the *B* and *A* positions. This is clear from the data listed in Table 8. Summarizing the results and taking into account the occupancies obtained from the above analysis, the formula of the ACB_2O_8 wodginite can be rewritten in the following way: $(Mn_{0.61}Ta_{0.39})Fe(Mn_{0.06}Ta_{0.58}Nb_{0.36})_2O_8$.

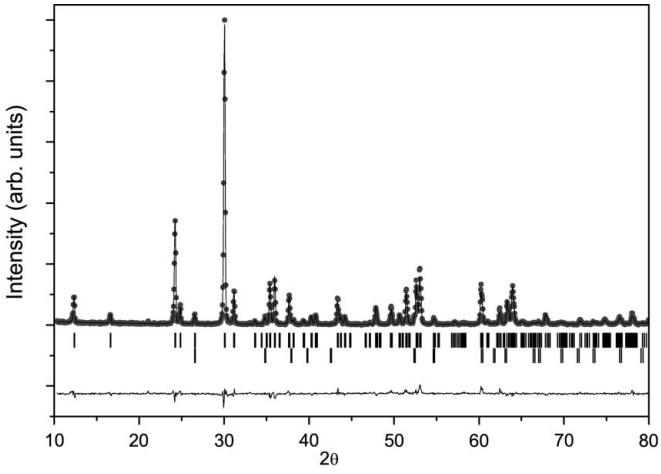

Figure 8
X-ray diffraction pattern recorded at room temperature for the sample heated in vacuum (V_{ac}). The points refer to the experimental data and the line to the Rietveld refinement fit. The Bragg peak positions corresponding to the columbite structure (*Pbcn*) are indicated by the first row of ticks; we also see the signatures of small amounts of rutile (second row of ticks).

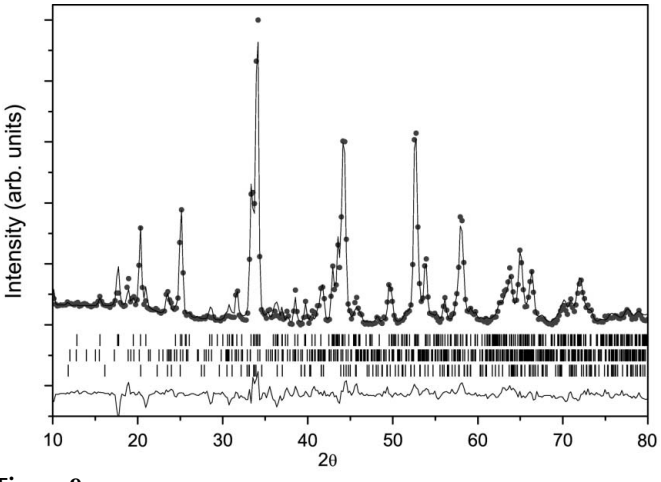

Figure 9
Rietveld refinement of the room-temperature neutron diffraction pattern recorded on the D1B instrument for the natural sample heated in air (A_{ir}). The points refer to the experimental data and the line to the Rietveld refinement fit. The first row of ticks correspond to the Bragg positions of the wodginite (*C*2/*c*) crystal structure, the second and third rows of ticks refer to the Ta_2O_5 (Lehovec, 1964) and Nb_2O_5 (Ercit, 1991) minority phases, respectively.

4. Conclusion

Using a combination of different techniques, we have determined *ab initio* the cation ordering of Ta, Nb, Fe and Mn atoms in the columbite and wodginite structure of the natural sample. The as-collected natural sample features cation disorder. It was found that the effect of annealing in vacuum induced a complete ordering of the Fe and Mn atoms on the *A* position of the AB_2O_6 crystal structure, whereas the Nb and Ta atoms are exclusively located on the *B* site. The sample heat treated in air presents a different crystal structure: indeed, the columbite phase transforms into the wodginite type as a consequence of the oxidation. In this case, this study has revealed that the crystal structure is not completely ordered following the annealing process used. The iron and manganese

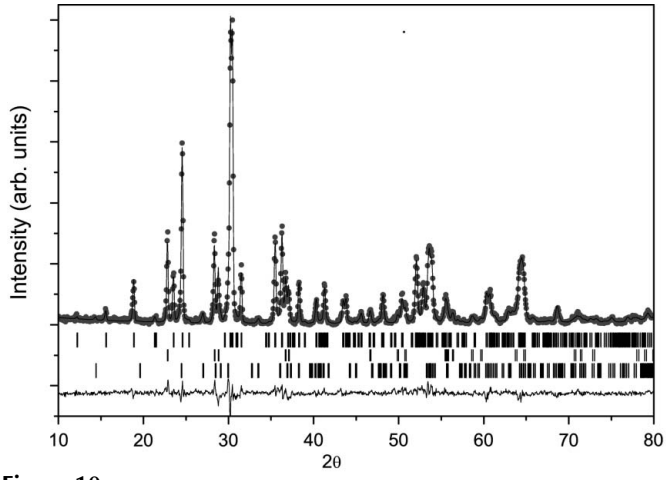

Figure 10
X-ray diffraction pattern recorded at room temperature for sample A_{ir} (heated in air). The points refer to the experimental data and the line to the Rietveld refinement fit. The first row of ticks corresponds to the Bragg positions of the wodginite (*C*2/*c*) crystal structure, the second and third rows of ticks refer to the Ta_2O_5 (Lehovec, 1964) and Nb_2O_5 (Ercit, 1991) minority phases, respectively.

atoms are found to prefer the *A* and *C* sites, whereas the Nb and Ta are preferentially located on the *B* site of the ACB_2O_8 wodginite phase.

This article is dedicated to the memory of V. Antonietti, who passed away before the end of his thesis work. We are grateful to D. Schmitt for a very interesting discussion. This work was supported in part by the French–Brazilian programme CAPES–COFECUB and the Brazilian agency CNPq. Financial support from the ARCUS Brésil cooperation program is also acknowledged.

References

Adusumilli, M. S. (1976). PhD thesis, Universidade Federal de Minas Gerais Brazil, Brazil.
Antonietti, V., Kinast, E. J., Zawislak, L. I., da Cunha, J. B. M. & dos Santos, C. A. (2001). *J. Phys. Chem. Solids*, **62**, 1239–1242.
Bancroft, G. M. (1973). *Mössbauer Spectroscopy. An Introduction for Inorganic Chemists and Geochemists.* London: McGraw–Hill.
Beurlen, H., da Silva, M. R. R., Thomas, R., Soares, D. R. & Olivier, P. (2008). *Miner. Deposita*, **43**, 207–228.
Cerny, P., Goad, B. E., Hawthorne, F. C. & Chapman, R. (1986). *Am. Mineral.* **71**, 501–517.
Drew, M. G. B., Hobson, R. J. & Padayatchy, V. T. (1993). *J. Mater. Chem.* **3**, 889–892.
Eibschüt, M., Ganiel, U. & Shtrikman, S. (1967). *Phys. Rev.* **156**, 259–261.
Eicher, S. M., Greedan, J. E. & Lushington, K. J. (1986). *J. Solid State Chem.* **62**, 220–230.
Ercit, T. S. (1991). *Miner. Petrol.* **43**, 217–223.
Ercit, T. S., Cerny, P., Hawthorne, F. C. & McCammon, C. A. (1992). *Can. Mineral.* **30**, 613–631.
Ercit, T. S., Wise, M. A. & Cerny, P. (1995). *Am. Mineral.* **80**, 613–619.
Esmaeilzadeh, S. & Grins, J. (2002). *Solid State Sci.* **4**, 117–123.
Felten, E. J. (1967). *Mater. Res. Bull.* **2**, 13–24.
Ferguson, R. B., Hawthorne, F. C. & Grice, J. D. (1976). *Can. Mineral.* **14**, 550–560.
Griffen, D. H. & Ribbe, P. H. (1979). *N. J. Mineral. Abh.* **137**, 54–73.
Hanawa, T., Shinkawa, K., Ishikawa, M., Miyatani, K., Saito, K. & Kohn, K. (1994). *J. Phys. Soc. Jpn*, **63**, 2706–2715.
Heid, C., Weitzel, H., Bourdarot, F., Calemczuk, R., Vogt, T. & Fuess, H. (1996). *J. Phys. Condens. Matter*, **8**, 10609.
Hutton, C. O. (1958). *Am. Mineral.* **43**, 112–119.
Kinast, E. J., Antonietti, V., Schmitt, D., Isnard, O., da Cunha, J. B., Gusmão, M. A. & dos Santos, C. A. (2003). *Phys. Rev. Lett.* **91**, 197208.
Kinast, E. J., dos Santos, C. A., Schmitt, D., Isnard, O., Gusmão, M. A. & da Cunha, J. B. M. (2010). *J. Alloys Compd.* **491**, 41–44.
Kinast, E. J., Zawislak, L. I., da Cunha, J. B. M., Antonietti, V., de Vasconcellos, M. A. Z. & dos Santos, C. A. (2002). *J. Solid State Chem.* **163**, 218–223.
Kobayashi, S., Mitsuda, S., Ishikawa, M., Miyatani, K. & Kohn, K. (1999). *Phys. Rev. B*, **60**, 3331–3345.
Kobayashi, S., Mitsuda, S. & Prokes, K. (2001). *Phys. Rev. B*, **63**, 024415.
Kremer, R. K. & Greedan, J. E. (1998). *J. Solid State Chem.* **73**, 579–582.
Lehovec, K. (1964). *J. Less Common Met.* **7**, 397–410.
Long, G. J., Cranshaw, T. E. & Longworth, G. (1983). *Mössbauer Effect Ref. Data J.* **6**, 42–49.
Mello, V. D., Zawislak, L. I., da Cunha, J. B. M., Kinast, E. J., Soares, J. B. & dos Santos, C. A. (1999). *J. Magn. Magn. Mater.* **196–197**, 846–847.
Muraoka, Y., Idogaki, T. & Uryu, N. (1988). *J. Phys. Soc. Jpn*, **57**, 1758–1761.
Nickel, E. H., Rowland, J. F. & McAdam, R. C. (1963). *Can. Mineral.* **7**, 390.
Oliveira Neto, S. R. de, Kinast, E. J., Gusmão, M. A., dos Santos, C. A., Isnard, O. & da Cunha, J. B. M. (2007). *J. Phys. Condens. Matter*, **19**, 356210.
Oliveira Neto, S. R. de, Kinast, E. J., Isnard, O., da Cunha, J. B. M., Gusmão, M. A. & dos Santos, C. A. (2008). *J. Magn. Magn. Mater.* **320**, E125–E127.
Pullar, R. C. (2009). *J. Am. Ceram. Soc.* **92**, 563–577.
Reimers, J. N., Greedan, J. E., Stager, C. V. & Kremer, R. (1989). *J. Solid State Chem.* **83**, 20–30.
Rodriguez-Carvajal, J. (1993). *Phys. B*, **192**, 55–69.
Santos, C. A. dos & Oliveira, J. (1992). *Solid State Commun.* **82**, 89–91.
Santos, C. A. dos, Zawislak, L. I., Antonietti, V., Kinast, E. J. & da Cunha, J. B. M. (1999). *J. Phys. Condens. Matter*, **11**, 7021–7033.
Santos, C. A. dos, Zawislak, L. I., Kinast, E. J., Antonietti, V. & da Cunha, J. B. M. (2001). *Braz. J. Phys.* **31**, 616–631.
Sarvezuk, P. W. C., Kinast, E. J., Colin, C. V., Gusmao, M. A., da Cunha, J. B. M. & Isnard, O. (2011). *Phys. Rev. B*, **83**, 174412.
Sears, V. F. (1992). *Neutron News*, **3**(3), 26–37.
Tarakina, N. V., Tyutyunnik, A. P., Zubkov, V. G., D'Yachkova, T. V., Zainulin, Y. G., Hannerz, H. & Svensson, G. (2003). *Solid State Sci.* **5**, 983–994.
Tarantino, S. C., Zema, M., Pistorino, M. & Domeneghitti, M. C. (2003). *Phys. Chem. Miner.* **30**, 590–598.
Turnock, A. C. (1966). *Can. Mineral.* **8**, 461–470.
Wenger, M., Armbruster, T. & Geiger, C. A. (1991). *Am. Mineral.* **76**, 1897–1904.
Wise, M. A. & Cerny, P. (1996). *Can. Mineral.* **34**, 631–647.
Wise, M. A., Turnock, A. C. & Cerny, N. (1985). *N. Jahrb. Miner. Monatsh.* **8**, 372–378.
Yeager, I., Morrish, A. H. & Wanklyn, B. M. (1977). *Phys. Rev. B*, **15**, 1465–1476.
Yeager, I., Morrish, A. H., Wanklyn, B. M. & Garrad, B. J. (1977). *Phys. Rev. B*, **16**, 2289–2299.
Zawislak, L. I., Antonietti, V., da Cunha, J. B. M. & dos Santos, C. A. (1997). *Solid State Commun.* **101**, 767–770.
Zawislak, L. I., da Cunha, J. B. M., Vasquez, A. & dos Santos, C. A. (1995). *Solid State Commun.* **94**, 345–348.